The Astrophysical Journal, 631:L113–L116, 2005 October 1

SPITZER IRAC IMAGING OF THE RELATIVISTIC JET FROM SUPERLUMINAL QUASAR PKS 0637−752

Yasunobu Uchiyama,[1] C. Megan Urry,[1] Jeffrey Van Duyne,[1] C. C. Cheung,[2,3] Rita M. Sambruna,[4] Tadayuki Takahashi,[5,6] Fabrizio Tavecchio,[7] and Laura Maraschi[7]

Received 2005 July 5; accepted 2005 August 25; published 2005 September 14

ABSTRACT

Emission from the relativistic jet located hundreds of kiloparsecs from the core of the superluminal quasar PKS 0637−752 was detected at 3.6 and 5.8 μm with the Infrared Array Camera (IRAC) on the *Spitzer Space Telescope*. The unprecedented sensitivity and arcsecond resolution of IRAC allows us to explore the mid-infrared emission from kiloparsec-scale quasar jets for the first time. The mid-infrared flux from the jet knots, when combined with radio and optical fluxes, confirms the synchrotron origin of the radio-to-optical emission and constrains very well the high-energy end of the nonthermal electron distribution. Assuming that the X-rays are produced in the relativistically moving knots via inverse Compton scattering of cosmic microwave background (CMB) radiation, the infrared observation puts constraints on the matter content of the large-scale quasar jet. Specifically, pure e^+e^- pair jet models are unfavorable based on the lack of an infrared bump associated with the "bulk Comptonization" of CMB photons by an ultrarelativistic jet.

Subject headings: galaxies: jets — infrared: galaxies — quasars: individual (PKS 0637−752) — radiation mechanisms: nonthermal

1. INTRODUCTION

Since the discovery of an X-ray jet of the quasar PKS 0637−752 (Chartas et al. 2000; Schwartz et al. 2000), a number of X-ray jets extending distances of hundreds of kiloparsecs from the quasar nucleus have been unveiled by *Chandra* (see, e.g., Sambruna et al. 2004 and Marshall et al. 2005). The X-ray emission mechanism, however, still remains unsettled for most of the large-scale jets of powerful quasars. Based on the spectral energy distribution (SED) from radio, optical, and X-ray bands, it has been argued that the X-ray intensity is too high to be explained by synchrotron or synchrotron self-Compton radiation from a single population of electrons.

A currently favored hypothesis for the strong X-ray emission is *relativistically amplified* inverse Compton (IC) scattering of the cosmic microwave background (CMB), in which the bulk flow of the jet is assumed to be relativistic, with a Lorentz factor $\Gamma \sim 10$ all the way to nearly megaparsec distances, and to be directed toward the observer at a small viewing angle of $\theta \sim \Gamma^{-1}$ (Tavecchio et al. 2000; Celotti et al. 2001). However, some difficulties in this model have been recognized, and alternative scenarios have been proposed (Aharonian 2002; Dermer & Atoyan 2002; Stawarz & Ostrowski 2002; Atoyan & Dermer 2004). Discussions of these models are hampered by the poorly known physical conditions in quasar jets as well as by the limited observational windows available so far.

In this Letter, we present *Spitzer* IRAC imaging at wavelengths 3.6 and 5.8 μm of the jet of the superluminal quasar PKS 0637−752. With the unprecedented sensitivity afforded by IRAC, the observation aimed at measuring the mid-infrared part of the broadband nonthermal spectrum of the jet knots. Also, we have searched for a possible infrared bump, which is expected if the jet is indeed highly relativistic at distances of hundreds of kiloparsecs from the central engine and if it contains cold (a Lorentz factor $\gamma \sim 1$) electrons. The redshift of PKS 0637−752 is $z = 0.651$ (Savage et al. 1976), so we adopt a luminosity distance of $D_L = 1.26 \times 10^{28}$ cm, for a ΛCDM cosmology with $\Omega_m = 0.27$, $\Omega_\Lambda = 0.73$, and $H_0 = 71$ km s^{-1} Mpc^{-1}.

2. OBSERVATIONS AND RESULTS

We have observed PKS 0637−752 with *Spitzer* IRAC on 2005 March 27 as part of our Cycle-1 General Observer program (*Spitzer* program ID 3586). IRAC is equipped with a 4-channel camera, InSb arrays at 3.6 and 4.5 μm, and Si:As arrays at 5.8 and 8.0 μm, each with a 5.′2 × 5.′2 field of view (Fazio et al. 2004). Only the pair of 3.6 and 5.8 μm arrays, observing the same sky simultaneously, was chosen for the observation of PKS 0637−752, to obtain longer exposures in one pair of bandpasses as opposed to two pairs with truncated exposure time. The 3.6/5.8 pair was chosen for a better spatial resolution and sensitivity. The pixel size in both arrays is $\simeq$1.″22. The point-spread functions are 1.″66 and 1.″88 (FWHM) for the 3.6 and 5.8 μm bands, respectively (Fazio et al. 2004). A total of 50 frames per IRAC band, each with a 30 s frame time, were obtained. The 50 images of the Basic Calibrated Data processed in the *Spitzer* Science Center (SSC) were combined into a projected image using the SSC software `mopex`.

Our aims are to explore possible infrared emission of the jet close (<12″) to the quasar core. For this purpose, the wings of the bright core must be subtracted carefully. We made use of the point-response function (PRF) image of a bright star provided by the SSC to cancel out the PRF wings. We also employed three bright field stars in our 3.6 μm image as PRF templates

[1] Yale Center for Astronomy and Astrophysics, Yale University, 260 Whitney Avenue, New Haven, CT 06520-8121; yasunobu.uchiyama@yale.edu, meg.urry@yale.edu, vanduyne@astro.yale.edu.

[2] Jansky Postdoctoral Fellow; National Radio Astronomy Observatory. Now hosted by Kavli Institute for Particle Astrophysics and Cosmology, Stanford University, Stanford, CA 94305.

[3] Massachusetts Institute of Technology, Kavli Institute for Astrophysics and Space Research, 77 Massachusetts Avenue, Cambridge, MA 02139; ccheung@space.mit.edu.

[4] Department of Physics and Astronomy and School of Computational Sciences, George Mason University, 4400 University Drive, Fairfax, VA 22030; rms@physics.gmu.edu.

[5] JAXA/ISAS, 3-1-1 Yoshinodai, Sagamihara, Kanagawa 229-8510, Japan; takahasi@astro.isas.jaxa.jp.

[6] Department of Physics, University of Tokyo, 7-3-1 Hongo, Bunkyoku, Tokyo 113-0033, Japan.

[7] Osservatorio Astronomico di Brera, via Brera 28, I-20121 Milan, Italy; tavecchio@merate.mi.astro.it, maraschi@brera.mi.astro.it.

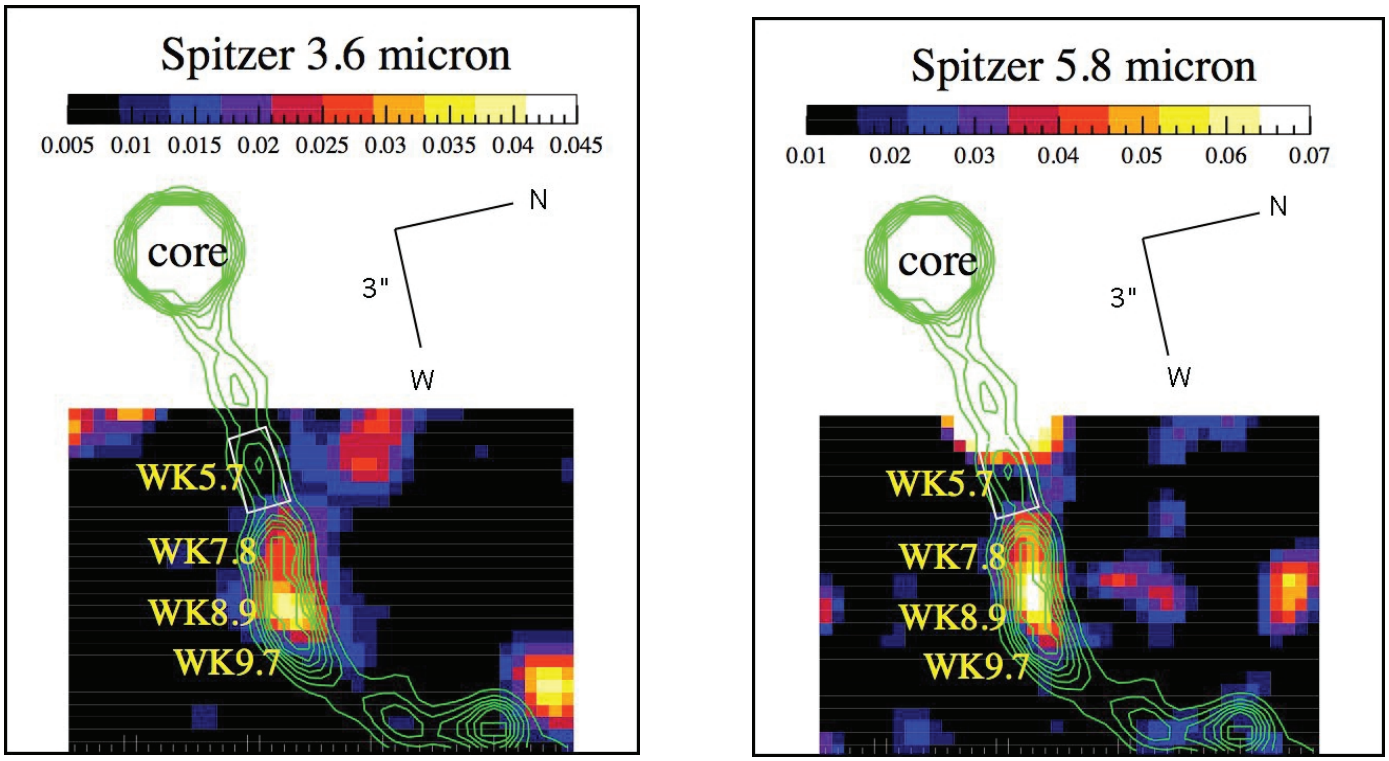

FIG. 1.—IRAC images (*false color*) of the PKS 0637−752 jet at 3.6 μm (*left*) and 5.8 μm (*right*) in units of MJy sr^{-1}. An angular scale of 1″ corresponds to a 6.9 kpc projected size. Superposed on the IRAC images are ATCA 8.6 GHz radio contours (using a circular restoring beam with 0.″88 FWHM), starting at 0.003 mJy beam^{-1} with an increment of 0.003 mJy beam^{-1} (Lovell et al. 2000). The emission east of WK5.7 in the 5.8 μm image is confused by residuals from wing cancellation.

and found that the results from the SSC template are consistent with those from the field star templates. In our 5.8 μm image, on the other hand, there are no suitable stars for such comparisons. In what follows, we present both the 3.6 and 5.8 μm results, making use of the SSC template alone. The infrared fluxes from the core of PKS 0637−752 were measured as 5.0 and 9.6 mJy in the 3.6 and 5.8 μm bands, respectively. These values are below the saturation limits for a 30 s frame.

Figure 1 shows the IRAC images of PKS 0637−752 after subtraction of the PRF wings of the core. The pixel size of the projected images of both channels was set to be $\frac{1}{4}$ of 1.″22. Regions close to the quasar core are blanked out due to residuals in the wing subtraction. Mid-infrared counterparts of the main optical knots, WK7.8 and WK8.9 (Schwartz et al. 2000), which are also the main X-ray features, are clearly visible in both channels, located ~8″ west of the core. The two optical knots

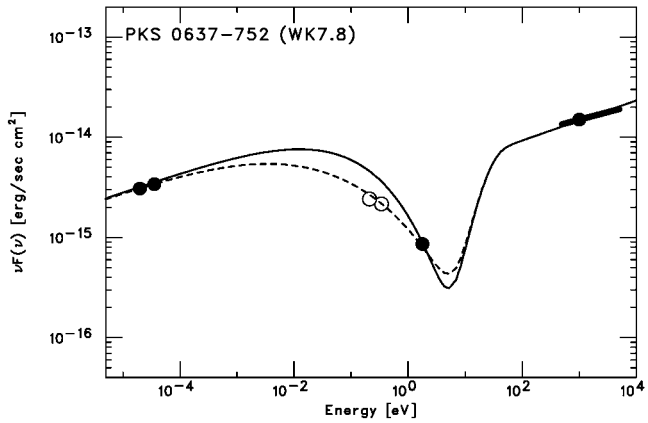

FIG. 2.—Broadband SED for knot WK7.8. IRAC 3.6 and 5.8 μm fluxes, 2.7 and 4.6 μJy, respectively, are shown as open circles. The radio flux at 8.6 GHz, 44 mJy, is extracted from the ATCA map centered on WK7.8 with a radius of 0.″8, while the 4.8 GHz flux is set to satisfy $\alpha_r = 0.8$. The *HST* optical (0.2 μJy at 697 nm) and *Chandra* X-ray data (6.2 nJy at 1 keV) are taken from the list of Kataoka & Stawarz (2005). The solid and dashed lines represent the synchrotron+IC/CMB modeling (see text).

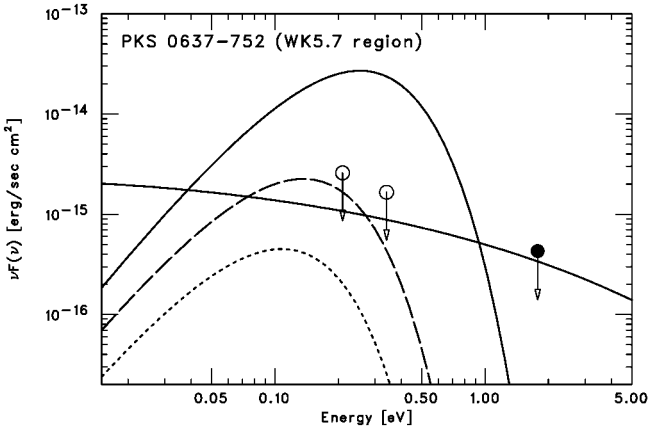

FIG. 3.—Bulk Comptonization spectra expected from the WK5.7 region (2″ long) assuming $L_{\rm cold} = 10^{46}$ ergs s^{-1} and (*a*) $\Gamma = 12$, $\theta = 3.^{\circ}5$ (*solid curve*), (*b*) $\Gamma = 12$, $\theta = 6.^{\circ}5$ (*dashed curve*), and (*c*) $\Gamma = 15$, $\theta = 8.^{\circ}3$ (*dotted curve*). Also shown is a synchrotron spectrum (*solid horizontal line*) extrapolated from the radio flux at 8.6 GHz with the spectral form of the dotted line in Fig. 2. The upper limits on IRAC 3.6 and 5.8 μm fluxes are shown as open circles. The optical upper limit is obtained from the 696.9 nm *HST* image (Schwartz et al. 2000).

TABLE 1
JET POWERS IN COLD AND NONTHERMAL ELECTRONS

Case	Γ	θ (deg)	δ	$L_{\rm cold}$ (ergs s^{-1})	$L_{\rm knot}$ (ergs s^{-1})	ξ ($=L_{\rm knot}/L_{\rm cold}$)	$n_{\rm cold}/n_e$	u_e/u_B
a	12	3.5	15.6	$<1.0 \times 10^{45}$	2.8×10^{45}	>2.8	<20	0.69
b	12	6.5	8.4	$<1.6 \times 10^{46}$	9.2×10^{46}	>5.8	<10	92
c	15	8.3	5.3	$<1.4 \times 10^{47}$	1.9×10^{48}	>14	<4	2.9×10^3

are marginally separated in the infrared images. In the 3.6 μm image, WK8.9 appears to be brighter than WK7.8, as in the optical. In the X-ray, WK8.9 is brighter than WK7.8, but the fluxes are more similar (Chartas et al. 2000). No significant infrared emission can be seen at WK5.7, WK9.7 (~3 times fainter than WK8.9 in the optical), or farther components after a bending point at ~10″ west of the quasar.

Photometry was performed with 5″ diameter apertures enclosing both WK7.8 and WK8.9, which finds $f_{3.6} = 6.5 \pm 0.5$ μJy and $f_{5.8} = 11 \pm 2$ μJy for 3.6 and 5.8 μm, respectively. The 1 σ errors include the uncertainties associated with PRF removal, adopting 10% of the quasar's wing intensity at the location being considered. Note that we measure the sum of infrared flux from the two optical knots. The infrared-to-optical slope[8] is $\alpha_{\rm io} \simeq 1.6$, significantly steeper than the spectral index at either radio or X-ray wavelengths, i.e., $\alpha_r = 0.81 \pm 0.01$ and $\alpha_{\rm X} = 0.85 \pm 0.08$ (Chartas et al. 2000).

Although the separation of the two knots is only $\simeq$1″, we can derive a rough flux ratio between WK7.8 and WK8.9 at the 3.6 μm band, thanks to the high significance and better PRF in this band. The flux from WK8.9 is higher by a factor of 1.5 ± 0.6 than WK7.8, in agreement with a factor of $\simeq$1.4 in the optical.

We can place upper limits on the IR fluxes from a "quiet" region preceding the nonthermal condensations WK7.8–8.9. For the white box in Figure 1 that encloses WK5.7, $f_{3.6} < 2$ μJy and $f_{5.8} < 5$ μJy (at a 2 σ level) are obtained. The flux uncertainty is computed as $2\sqrt{N}\sigma$, where N are the "noise pixels" taken from Fazio et al. (2004) and σ presents the background noise in which PRF-removal uncertainty is also formally included. We use these flux limits later in § 3.2.

3. DISCUSSION

3.1. *SED of Knot WK7.8*

The mid-infrared fluxes that we have measured fill central points in the SED of the jet knots and, therefore, set an important constraint on models of the broadband emission. In Figure 2, we show the SED for knot WK7.8, the first bright knot that has been frequently modeled in the literature. The knot is unresolved both in the radio image (Australia Telescope Compact Array [ATCA]) and the *Hubble Space Telescope* (*HST*) image (Schwartz et al. 2000). Also, the corresponding knot is visible in the deconvolved *Chandra* X-ray image (Chartas et al. 2000). The emissions in these bands most likely emerge from the same physical volume. (In contrast, knot WK8.9 appears elongated along the jet in the optical, and so may involve multiple knots.) Setting a flux ratio in the infrared between WK7.8 and WK8.9 to be 1.4 based on the optical (see above), we associate flux densities of 2.7 μJy (3.6 μm) and 4.6 μJy (5.8 μm) with knot WK7.8.

The radio-to-optical spectrum is now arguably attributable to synchrotron radiation, because the extrapolation of the radio spectrum can smoothly connect with the infrared and optical fluxes assuming normal steepening due to radiative cooling. Specifically, we first assume that the energy distribution of the electrons (in the jet comoving frame) follows $N(\gamma) = K\gamma^{-s}\exp(-\gamma/\gamma_{\rm max})$ for $\gamma > \gamma_{\rm min}$, where K is the normalization, γ denotes the Lorentz factor of relativistic electrons, and $s = 2.6$ to match the radio slope $\alpha \simeq 0.8$ ($s = 2\alpha + 1$). To reproduce the optical flux, we obtain $\gamma_{\rm max} \simeq 3.6 \times 10^5(\delta_{10}B_{-5})^{-1/2}$, where $\delta_{10} = \delta/10$ and $B_{-5} = B/(10^{-5}$ G) are the characteristic Doppler factor[9] and comoving magnetic field strength (the solid line in Fig. 2). The low-energy cutoff $\gamma_{\rm min}$ is arbitrary as long as $\gamma_{\rm min} < 2 \times 10^3(\delta_{10}B_{-5})^{-1/2}$.

This simple model for the synchrotron component overpredicts the mid-infrared flux by a factor of ~2. To account for this discrepancy, we modified the form of the electron distribution to $N(\gamma) = K\gamma^{-s}(1+\gamma/\gamma_{\rm br})^{-1}\exp(-\gamma/\gamma_{\rm max})$ with $s = 2.6$, which is a smooth broken power law with an exponential cutoff, taking account of possible synchrotron and IC (in the Thomson regime) cooling. Fitting the SED with this model, we obtain $\gamma_{\rm br} \simeq 1.4 \times 10^5(\delta_{10}B_{-5})^{-1/2}$ and $\gamma_{\rm max} \simeq 1.1 \times 10^6(\delta_{10}B_{-5})^{-1/2}$ (the dashed line in Fig. 2).

Here we also model the X-ray spectrum, for illustrative purposes, by the IC/CMB model (Tavecchio et al. 2000), namely, by the model invoking relativistically amplified IC scattering on CMB radiation, with the Doppler factor of $\delta = 8.4$ (corresponding to case *b* in § 3.2) and $\gamma_{\rm min} = 20$. In order to support the X-ray flux and at the same time to suppress the optical flux by the IC process, we obtain a tight constraint, $10 \lesssim \gamma_{\rm min} \lesssim 40$. Note that the IC/CMB model for the X-rays generally requires large power carried by nonthermal relativistic electrons, $L_{\rm knot} \simeq \pi r^2\Gamma^2\beta c u_e$, where $r = 1$ kpc is the adopted radius of the knot and u_e is the energy density of nonthermal electrons in the jet frame, which can be written as $u_e = \langle\gamma\rangle m_e c^2 n_e = [(p-1)/(p-2)]\gamma_{\rm min} m_e c^2 n_e$, with n_e being the number density of nonthermal electrons. For example, one needs $L_{\rm knot} \sim 9.2 \times 10^{46}$ ergs s^{-1} in the case of the parameter set (case *b*) in § 3.2 ($\delta = 8.4$, $\Gamma = 12$, and $\gamma_{\rm min} = 20$).

The detected mid-infrared fluxes well constrain the highest energy part of the electron distribution, say, $\gamma \sim 10^5$–10^6. In addition, as we show below, the *nondetection* of infrared light from the jet preceding WK7.8 strongly constrains the lowest energy ($\gamma \sim 1$) electrons, which have yet to be accelerated.

3.2. *Bulk Compton Radiation*

The relativistically amplified IC/CMB scenario raises the interesting possibility that an infrared bump may appear as a result of "bulk Comptonization" (BC), namely, Comptonization of the CMB photons by "cold" ($\gamma \sim 1$) electrons or positrons in the ultrarelativistic jet stream (Sikora et al. 1997; Georganopoulos et al. 2005). The BC bump is expected to have a blackbody-like

[8] We define $\alpha_{\rm io} \equiv -\log(f_{\rm ir}/f_{\rm op})/\log(\nu_{\rm ir}/\nu_{\rm op})$, with $\nu_{\rm ir} = 0.83 \times 10^{14}$ Hz (for 3.6 μm) and $\nu_{\rm op} = 4.3 \times 10^{14}$ Hz. We take $f_{\rm ir} = 6.5$ μJy and $f_{\rm op} = 0.48$ μJy (Schwartz et al. 2000).

[9] The Doppler factor is defined as $\delta \equiv [\Gamma(1-\beta\cos\theta)]^{-1}$, where βc the velocity of the jet, $\Gamma = (1-\beta^2)^{-1/2}$ is the bulk Lorentz factor of the jet, and θ is the observing angle with respect to the jet direction.

spectrum peaking at the energy $\epsilon_{\rm BC} \simeq 2\delta\Gamma\epsilon_{\rm CMB}$, independent of redshift, where $\epsilon_{\rm CMB}$ is the mean energy of the CMB radiation at $z = 0$. For $\Gamma = \delta = 10$, the bump appears at the infrared wavelength $\lambda_{\rm BC} \sim 10$ μm. The isotropic BC luminosity from a relativistic jet containing cold electrons, assuming a cylindrical geometry of radius r and length $l_{\rm cold}$, is given by (Georganopoulos et al. 2005)

$$L_{\rm BC} \simeq \frac{4}{3}\frac{\sigma_{\rm T}}{m_e c^2} l_{\rm cold} U_{\rm CMB} \beta\delta^3 L_{\rm cold}, \quad (1)$$

where $\sigma_{\rm T}$ is the Thomson cross section, $U_{\rm CMB} = 4.2 \times 10^{-13}(1+z)^4$ ergs cm^{-3}, and $L_{\rm cold}$ is the jet power carried by cold electrons that upscatter CMB radiation into the infrared, defined as $L_{\rm cold} = \pi r^2 \Gamma^2 \beta c n_{\rm cold} m_e c^2$, with $n_{\rm cold}$ being the number density of cold electrons in the jet frame.

Along a "quiet" stream between the core and the first bright knot WK7.8, it is expected that unseen cold particles are propagating and generating BC radiation. In Figure 3, we present BC spectra calculated for the quiet portion of the jet, assuming for illustrative purposes that $L_{\rm cold} = 10^{46}$ ergs s^{-1}. The length of this region is set to be $l_{\rm cold} = (13.8/\sin\theta)$ kpc, which is appropriate for the white box in Figure 1, where the flux upper limits were derived in § 2. We consider the three characteristic cases as follows: (*a*) $\Gamma = 12$, $\theta = 3\overset{\circ}{.}5$, (*b*) $\Gamma = 12$, $\theta = 6\overset{\circ}{.}5$, and (*c*) $\Gamma = 15$, $\theta = 8\overset{\circ}{.}3$. These parameters are chosen for the consistency with the VSOP and VLBI observations, which found superluminal motions on milliarcsecond scales (~100 pc distances from the core) with a mean apparent speed of $\beta_{\rm app} c = 11.4c \pm 0.6c$, indicating $\Gamma > 11.4$ (Lovell et al. 2000). The viewing angles are set by the well-known relation (see Urry & Padovani 1995) $\beta_{\rm app} = \beta\sin\theta/(1-\beta\cos\theta)$, with $\beta_{\rm app} = 11.4$, which yields two solutions for a given Γ. For $\Gamma = 15$, the smaller angle solution $\theta = 1\overset{\circ}{.}8$ requires an unlikely long jet, exceeding a deprojected total length of 2.2 Mpc, and therefore is omitted. From Figure 3, one can constrain $L_{\rm cold}$ by comparing the calculated BC spectra to the flux upper limits obtained from the IRAC data. The results are summarized in Table 1.

In Table 1, the jet power in nonthermal electrons, $L_{\rm knot}$, is given based on the IC/CMB modeling of knot WK7.8 (with $\gamma_{\rm min} = 20$), together with the lower limits on $\xi \equiv L_{\rm knot}/L_{\rm cold} = \langle\gamma\rangle n_e/n_{\rm cold}$. The ratio of the energy densities of nonthermal electrons u_e and magnetic fields u_B is also shown. It appears that case *c* has uncomfortably large $L_{\rm knot}$ and u_e/u_B because of small δ (see also Dermer & Atoyan 2004).

The limits on $L_{\rm cold}$ impose meaningful constraints on the jet models. If the jet is dynamically dominated by e^+e^- pairs, one can assume that the energy flux of nonthermal electrons at the knot is stored in cold e^+e^- pairs before the first knot; therefore, $\xi \le 1$ (i.e., $L_{\rm cold} \ge L_{\rm knot}$). However, we obtain $\xi > 1$ for all cases (see Table 1). An estimate of ξ cannot be noticeably reduced by increasing $\gamma_{\rm min}$ (through the relation $L_{\rm knot} \propto \gamma_{\rm min}^{-0.6}$) as $\gamma_{\rm min} \lesssim 40\delta_{10}^{-1}$ is set by the X-ray spectrum. Also, changing θ in a plausible range $3° \le \theta \le 9°$ for both $\Gamma = 12$ and 15 does not affect our conclusion in this regard. Therefore, as long as the IC/CMB scenario is correct, our result argues against pure e^+e^- jet models.

Interestingly, *on subparsec scales* in radio-loud quasars, a similar conclusion has been reached by Sikora & Madejski (2000) that jet composition with pure e^+e^- pairs can be excluded by the absence of BC radiation at X-ray energies due to Comptonization of UV photons. The present work is the first time that jet composition on scales of many kiloparsecs has been constrained in this way.

The number density of cold electrons relative to that of nonthermal electrons can be constrained as $n_{\rm cold}/n_e < 4$–20 (see Table 1), by the relation $\xi = \langle\gamma\rangle n_e/n_{\rm cold}$ and $\langle\gamma\rangle \simeq 2.7\gamma_{\rm min} \sim 50$. We note that these limits are difficult to explain within the standard picture of particle acceleration, namely, diffusive shock acceleration, in which it is generally expected that only a small fraction of the cold electrons can be accelerated to nonthermal energies, and consequently $n_{\rm cold}/n_e \gg 1$. One may need to invoke alternative models regarding the X-ray emission mechanism (namely, IC/CMB) and/or the acceleration mechanism.

A possible caveat is that the above discussion relies on the simplified picture that the power transported by the jet is constant. If the ejection of power at the base of the jet is discontinuous, the emission knots may represent "power peaks," and the average jet power could be smaller than the value of $L_{\rm knot}$ that we calculated. It should also be noted that in our calculations of the BC spectra, we have assumed monoenergetic cold electrons of $\gamma = 1$. If instead a certain fraction of pairs is "hot" with γ of a few, the BC spectrum can be practically different from our calculation, extending to optical energies. Even so, the limits on $L_{\rm cold}$ would be similar to, or tighter than, what we obtained above.

We are grateful to Jim Lovell for providing us with the ATCA 8.6 GHz radio image. We would like to thank the anonymous referee for very helpful comments. This work was supported in part by NASA grant NAG5-12873. This work is based on observations made with the *Spitzer Space Telescope*, which is operated by the Jet Propulsion Laboratory, California Institute of Technology, under NASA contract 1407. Support for this work was provided by NASA through contract RSA 1265389 issued by JPL/Caltech.

Facilities: Spitzer(IRAC)

REFERENCES

Aharonian, F. A. 2002, MNRAS, 332, 215
Atoyan, A. M., & Dermer, C. D. 2004, ApJ, 613, 151
Celotti, A., Ghisellini, G., & Chiaberge, M. 2001, MNRAS, 321, L1
Chartas, G., et al. 2000, ApJ, 542, 655
Dermer, C. D., & Atoyan, A. M. 2002, ApJ, 568, L81
———. 2004, ApJ, 611, L9
Fazio, G., et al. 2004, ApJS, 154, 10
Georganopoulos, M., Kazanas, D., Perlman, E., & Stecker, F. W. 2005, ApJ, 625, 656
Kataoka, J., & Stawarz, Ł. 2005, ApJ, 622, 797
Lovell, J. E. J., et al. 2000, in Astrophysical Phenomena Revealed by Space VLBI, ed. H. Hirabayashi, P. G. Edwards, & D. W. Murphy (Sagamihara: ISAS), 215
Marshall, H. L., et al. 2005, ApJS, 156, 13
Sambruna, R. M., Gambill, J. K., Maraschi, L., Tavecchio, F., Cerutti, R., Cheung, C. C., Urry, C. M., & Chartas, G. 2004, ApJ, 608, 698
Savage, A., Browne, I. W. A., & Bolton, J. G. 1976, MNRAS, 177, 77P
Schwartz, D. A., et al. 2000, ApJ, 540, L69
Sikora, M., & Madejski, G. 2000, ApJ, 534, 109
Sikora, M., Madejski, G., Moderski, R., & Poutanen, J. 1997, ApJ, 484, 108
Stawarz, Ł., & Ostrowski, M. 2002, ApJ, 578, 763
Tavecchio, F., Maraschi, L., Sambruna, R. M., & Urry, C. M. 2000, ApJ, 544, L23
Urry, C. M., & Padovani, P. 1995, PASP, 107, 803